TECHNICAL REPORTS

nature medicine

A humanized bone marrow ossicle xenotransplantation model enables improved engraftment of healthy and leukemic human hematopoietic cells

Andreas Reinisch[1–3], Daniel Thomas[1–3], M Ryan Corces[1–3], Xiaohua Zhang[1–3], Dita Gratzinger[4], Wan-Jen Hong[1–3], Katharina Schallmoser[5,6], Dirk Strunk[6,7] & Ravindra Majeti[1–3]

Xenotransplantation models represent powerful tools for the investigation of healthy and malignant human hematopoiesis. However, current models do not fully mimic the components of the human bone marrow (BM) microenvironment, and they enable only limited engraftment of samples from some human malignancies. Here we show that a xenotransplantation model bearing subcutaneous humanized ossicles with an accessible BM microenvironment, formed by *in situ* differentiation of human BM-derived mesenchymal stromal cells, enables the robust engraftment of healthy human hematopoietic stem and progenitor cells, as well as primary acute myeloid leukemia (AML) samples, at levels much greater than those in unmanipulated mice. Direct intraossicle transplantation accelerated engraftment and resulted in the detection of substantially higher leukemia-initiating cell (LIC) frequencies. We also observed robust engraftment of acute promyelocytic leukemia (APL) and myelofibrosis (MF) samples, and identified LICs in these malignancies. This humanized ossicle xenotransplantation approach provides a system for modeling a wide variety of human hematological diseases.

Over the past several decades, a number of progressively more-immunodeficient mice strains have been developed. For example, the generation of NSG mice, which bear a targeted deletion of the interleukin (IL)-2 receptor, gamma chain (*Il2rg*) on the NOD-SCID background, enables the engraftment of many human solid tumors and hematopoietic malignancies[1]. However, even in NSG mice, the level of engraftment of human cells is often low, prompting the development of mouse strains that overexpress or that have targeted insertions of genes encoding human cytokines such as SCF, GM-CSF, IL-3, and TPO[2–5].

These mouse strains have been used extensively for the engraftment of human hematopoietic malignancies, particularly AML[6]. However, a large proportion of samples from patients with AML—in particular, the less aggressive subtypes such as those bearing mutations in core binding factors and those that are classified as APL—fail to engraft in NSG mice or do so at low levels that do not mimic human disease[7–9]. Additionally, some other hematopoietic neoplasms do not engraft at all in the currently available mouse strains. Attempts to generate xenograft models of myelodysplastic syndrome (MDS), myeloproliferative neoplasms (MPNs), and multiple myeloma have met with limited success[10–12], although a recent study used a modified NSG engraftment assay involving the co-transplantation of patient-derived mesenchymal stromal cells (MSCs) with their corresponding hematopoietic stem and progenitor cells (HSPCs) to identify MDS-initiating cells[13]. The reasons for the difficulty in engrafting some human hematopoietic neoplasms in mice remain largely unclear, but probably relate to species-specific requirements for environmental factors that mediate hematopoietic cell homing, survival, and expansion.

Hematopoiesis occurs primarily in the BM, where HSCs are localized in specialized microenvironments known as BM niches. In these niches, HSCs reside in close contact and engage in bidirectional interactions with a complex network of cells, including MSCs, osteoblasts, adipocytes, vascular endothelial cells, and Schwann cells[14]. These niches are also co-opted by leukemia cells in hematopoietic malignancies and can support leukemia stem cell (LSC) survival[15,16].

Recently, we reported that immature mesenchymal stromal cells from human BM (BM-MSCs), when mixed with extracellular matrix and implanted subcutaneously into the flanks of NSG mice, form a humanized BM microenvironment that is capable of recruiting and supporting the engraftment of mouse hematopoiesis. These ectopic humanized BM niches are also capable of recruiting various human mature blood cell lineages and $CD34^+$ (HSPCs) when human hematopoiesis was established before niche formation[17]. Given that primary malignant hematopoietic cells are dependent on proper BM-niche interactions[18], we speculated that providing a humanized microenvironment with a supply of human niche factors, as compared to unmanipulated NSG mouse BM, would be sufficient to facilitate superior engraftment and the growth of malignant human hematopoietic cells. Here we show that this is indeed the case: human BM-MSC-derived

[1]Division of Hematology, Department of Medicine, Stanford University School of Medicine, Stanford, California, USA. [2]Cancer Institute, Stanford University School of Medicine, Stanford, California, USA. [3]Institute for Stem Cell Biology and Regenerative Medicine, Stanford University School of Medicine, Stanford, California, USA. [4]Department of Pathology, Stanford University School of Medicine, Stanford, California, USA. [5]Department of Blood Group Serology and Transfusion Medicine, Paracelsus Medical University, Salzburg, Austria. [6]Spinal Cord Injury and Tissue Regeneration Center Salzburg, Paracelsus Medical University, Salzburg, Austria. [7]Experimental and Clinical Cell Therapy Institute, Paracelsus Medical University, Salzburg, Austria. Correspondence should be addressed to R.M. (rmajeti@stanford.edu).

Received 2 July 2015; accepted 6 April 2016; published online 23 May 2016; doi:10.1038/nm.4103

ossicles (ectopic bone organoid composed of human bone, stroma and hematopoietic tissue), when compared to unmanipulated NSG mouse BM, enable robust and superior engraftment of hematopoietic cells from patients with acute leukemias and other hematopoietic disorders.

RESULTS

Human HSPCs engraft in human BM-MSC-derived ossicles

To establish a xenotransplantation system for healthy and malignant human hematopoietic cells, we generated humanized BM niches in NSG mice *in vivo*[17] (**Fig. 1a** and **Supplementary Fig. 1a–f**, for a detailed protocol for humanized ossicle formation). Subcutaneous transplantation of human BM-MSCs, admixed with extracellular matrix (up to four transplants per mouse), results in the formation of a humanized BM microenvironment within an ossicle after 8–10 weeks. Transplanted cells undergo endochondral ossification *in situ* and form a marrow cavity, with concomitant invasion of mouse hematopoietic tissue, as indicated by a visible dark-purple color change (**Fig. 1a** and **Supplementary Fig. 1e**, left). The daily administration of an anabolic dose of human parathyroid hormone (40 μg/kg) for 28 d after BM-MSC transplantation resulted in a significant increase in the weight of the humanized ossicles, as compared to untreated mice (mean ± s.d.; 121.9 ± 35.6 mg versus 74.9 ± 29.6 mg; $P < 0.001$, **Supplementary Fig. 1f**)[19,20]. To confirm the human origin of ossicle bone and stromal niche elements, BM-MSCs were transduced with lentivirus encoding green fluorescent protein (GFP). Fluorescence microscopy revealed GFP$^+$ cells residing both within the bone structures and within the marrow space of mature ossicles (**Supplementary Fig. 1h**). 8–10 weeks after subcutaneous implantation, when hematopoietic areas were detectable within the ossicle by visual inspection (development of a purple hue within the ossicle; **Supplementary Fig. 1e**, left), ossicle-bearing NSG mice were conditioned with sublethal irradiation, and human hematopoietic cells were injected either intravenously or transcutaneously directly into the ossicle (**Fig. 1a** and **Supplementary Fig. 1e**,**f**). Because of the easily accessible subcutaneous location, human hematopoietic engraftment in the ossicles can be monitored by serial aspiration and flow cytometry, and histologic assessments performed at the time that the mice are euthanized (**Fig. 1a** and **Supplementary Fig. 1e**,**f**).

To investigate whether the humanized niches can support human hematopoiesis, we first performed intravenous transplantation of human cord-blood-derived CD34$^+$ HSPCs in mice bearing ossicles. In separate mice, we performed direct intraossicle injection into one ossicle of up to four per mouse. Independently of the transplantation route or the human donor, human CD45$^+$ cells, including both CD19$^+$ lymphoid cells and CD33$^+$ myeloid cells, were detected in the humanized ossicles as early as 4 weeks after transplantation (**Supplementary Fig. 2a**). Subsequent aspirates taken at 7–8 weeks and 17–18 weeks after transplantation revealed clear engraftment of human hematopoietic cells in all ossicles analyzed (**Fig. 1b**,**c** and **Supplementary Fig. 2b**). Human engraftment levels were higher in directly injected ossicles than in the BM of mice that received CD34$^+$ HSPCs through intravenous transplantation (mean ± s.d.; 7–8 weeks, 86.0 ± 9.6% versus 21.2 ± 26.3%; $P = 0.1$; 17–18 weeks, 90.1 ± 11.6% versus 52.1 ± 26.6%; $P = 0.06$) (**Fig. 1c**). Human engraftment levels were also significantly higher in directly injected ossicles than in the noninjected ossicles or the BM of the same mice, whose engraftment was indicative of homing of HSPCs from the injected ossicle to additional sites of hematopoietic niches (mean ± s.d.; 7–8 weeks, 86.0 ± 9.6% versus 21.3 ± 26.5%; $P < 0.001$, 86.0 ± 9.6% versus 23.5 ± 32.3%; $P < 0.05$; 17–18 weeks, 90.1 ± 11.6% versus 51.3 ± 28.0%; $P < 0.05$, 90.1 ± 11.6% versus 39.9 ± 22.8%; $P < 0.05$) (**Fig. 1c**). Finally, 17–18 weeks after the intravenous transplantation of human HSPCs, engraftment was higher in humanized niches than in mouse BM (mean ± s.d.; 70.7 ± 27.3% versus 52.1 ± 26.8%; $P < 0.05$) (**Fig. 1c**).

At 17–18 weeks after transplantation, we identified mature neutrophils, eosinophils, monocytes, mast cells, and conventional and plasmacytoid dendritic cells, as well as low levels of T cells (<4%), natural killer (NK) cells (<0.2%) and variable numbers of cells committed to the megakaryocyte lineage as well as nucleated-erythroid precursors, in the humanized ossicle niches. As expected, the majority of B cells in the ossicles were immature B cell precursors, and the mature B cells were polyclonal for the expression of immunoglobulin light chains kappa and lambda (**Supplementary Fig. 2c–g**).

Humanized ossicle niches retained and maintained human HSPC populations, including HSCs, multipotent progenitors (MPPs), lymphoid-primed multipotent progenitors (L-MPPs), common myeloid progenitors (CMPs), granulocyte-macrophage progenitors (GMPs), and megakaryocyte-erythroid progenitors (MEPs), for up to 23 weeks (**Supplementary Fig. 2h**,**i**). Finally, the presence of functional, self-renewing HSCs within the ossicles was confirmed by the successful engraftment of ossicle-derived cells in secondary recipients with and without established humanized ossicles (**Supplementary Fig. 2j**).

Leukemia cells engraft in human BM-MSC-derived ossicles

Next, we investigated the engraftment of primary human acute leukemia cells, both AML and acute lymphoblastic leukemia (ALL), through direct intraossicle injection (see **Supplementary Tables 1** and **2** for patient sample information). In the first case, we directly injected 10,000 AML blasts into each ossicle and tracked leukemia engraftment in the transplanted ossicle, as well as in the corresponding mouse BM. Transplanted ossicles exhibited a high level of leukemic engraftment at 12 weeks after transplantation, with >95% CD45^{low}CD33$^+$ leukemic blasts in all ossicles, and leukemic egress from the humanized ossicles led to a high burden of leukemia in the mouse BM (**Fig. 1d**,**e**). Intraossicle transplantation of a diverse cohort of AML samples demonstrated leukemia engraftment in 13 of 15 samples, with 12 out of 13 achieving >95% human leukemic chimerism in the transplanted ossicles (**Table 1**). Moreover, the intravenous transplantation of ossicle-bearing mice led to >80% leukemic engraftment in the ossicles for four of four AML samples (**Table 1**). In addition to AML, both patient-derived B cell ALL (B-ALL) and T cell ALL (T-ALL) cells engrafted at high levels in the ossicles after 8–11 weeks; eventually, the BM of mice that had received injections was completely taken over by human CD45$^+$CD19$^+$ cells or by CD45$^+$CD3$^+$ cells, respectively (**Fig. 1d**,**e**).

The high frequency and level of engraftment upon direct intraossicle injection suggests that the humanized ossicle niches are superior to mouse BM for the engraftment of human AML. To make direct comparisons, we identified four samples that engrafted poorly upon intravenous transplantation into unmanipulated NSG mice, with either low chimerism or delayed kinetics (**Table 1**). 1×10^6 primary AML blasts from each of these samples were either (i) directly injected into one ossicle per mouse, (ii) transplanted intravenously into mice bearing up to four ossicles, or (iii) transplanted intravenously into unmanipulated NSG mice (**Fig. 2a**). The kinetics and burden of CD45$^+$CD33$^+$ leukemia cell engraftment were evaluated by flow cytometry in all ossicles and in the mouse BM every 4–6 weeks, starting at 8 weeks after transplantation (**Fig. 2a**,**b** and **Supplementary Figs. 3** and **4**). At 8 weeks post-transplantation, a high leukemia burden

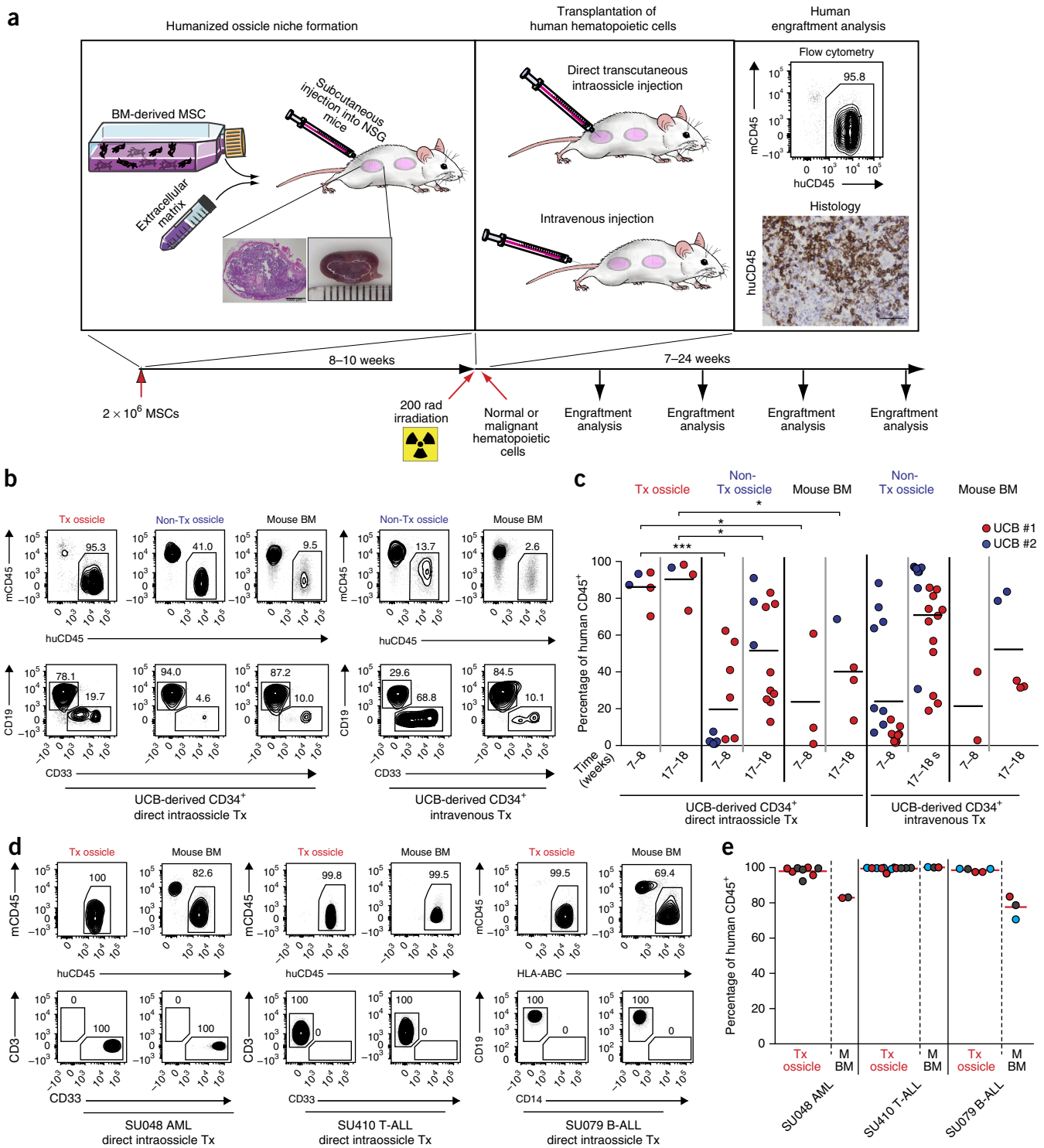

Figure 1 Human HSPCs and primary acute leukemia engraft robustly in human BM-MSC-derived ossicles. (**a**) Experimental schematic and time line. (**b**,**d**) Representative FACS plots showing human healthy (**b**) and leukemic (**d**) engraftment at the indicated time points after cell transplantation. (n = 2–20 per group). 1 × 10^4 UCB-derived CD34$^+$ HSPCs, 10,000 AML blasts (SU048), 1 × 10^5 T-ALL blasts (SU410), and 8.3 × 10^5 B-ALL blasts (SU079) were transplanted either intravenously (**b**, right) or directly into one of four ossicles (**b**, left, **d**). Transplanted (Tx) ossicle, nontransplanted (non-Tx) ossicles, and mouse BM were analyzed by flow cytometry for the presence of human healthy or leukemic CD45$^+$ cells. Engrafted healthy cells were further gated for myeloid cells (CD45$^+$CD33$^+$) and B lymphoid cells (CD45$^+$CD19$^+$). Leukemia engraftment was confirmed by exclusive expression of CD33 (SU048, AML), CD3 (SU410, T-ALL) and CD19 (SU079, B-ALL). (**c**,**e**) Summary of human chimerism levels in ossicles and mouse BM. (**c**) Dots represent individual engrafted ossicles at the indicated time points after transplantation. (Tx ossicle after direct intraossicle Tx, 7–8 weeks, n = 5; 17–18 weeks, n = 4; non-Tx ossicle after direct intraossicle Tx, 7–8 weeks, n = 13; 17–18 weeks, n = 12; mouse BM after direct intraossicle Tx, 7–8 weeks, n = 3; 17–18 weeks, n = 4; Tx ossicle after intravenous Tx, 7–8 weeks, n = 19; 17–18 weeks, n = 20; mouse BM after direct intraossicle Tx, 7–8 weeks, n = 2; 17–18 weeks, n = 5). *P < 0.05; ***P < 0.001, Mann–Whitney U test. All analyzed tissues were included in the analysis. (**e**) Each dot represents one separately transplanted ossicle (AML, n = 8; T-ALL, n = 12; B-ALL, n = 5) or mouse (AML, n = 2; T-ALL, n = 3; B-ALL, n = 3). Lines represent mean engraftment levels; colors represent different mice.

Table 1 Summary of engraftment assays of primary transplanted AML samples

Sample ID	Specimen type	WHO classification	Number of transplanted cells	Engraftment in ossicles (i.o. Tx) (mean ± s.d., time after Tx)	Engraftment in ossicles (i.v. Tx) (mean ± s.d., time after Tx)	Engraftment i.v. Tx (no ossicles) (mean ± s.d., time after Tx) No. of transplanted cells
SU306	pB	AML n.o.s.	1×10^6 MNCs (T cell depleted)	97.6 ± 1.5 (24 weeks)	96.9 ± 1.6 (24 weeks)	2.1. ± 1.9 (18 weeks) 1×10^6 MNCs (T cell depleted)
SU480	pB	AML n.o.s.	0.9×10^6 MNCs (T cell depleted)	97.8 ± 2.3 (22 weeks)	80.1 ± 18.5 (22 weeks)	31.6 ± 25.0 (18 weeks) 1×10^6 MNCs (T cell depleted)
SU532	pB	AML n.o.s.	1×10^6 MNCs (T cell depleted)	99.5 ± 0.7 (18 weeks)	98.4 ± 1.1 (18 weeks)	12.2 ± 23.3 (18 weeks) 1×10^6 MNCs (T cell depleted)
SU582	pB	AML n.o.s.	1×10^6 MNCs (T cell depleted)	98.1 ± 2.6 (18 weeks)	88.8 ± 12.8 (18 weeks)	5.4 ± 4.3 (18 weeks) 1×10^6 MNCs (T cell depleted)
SU490	pB	APL with *PML–RARA*	1×10^6 MNCs (T cell depleted)	97.4 ± 1.9 (15 weeks)	n.d.	2.2 ± 1.8 (18 weeks) 1×10^6 MNCs (T cell depleted)
SU589	pB	APL with *PML–RARA*	1.4×10^6 MNCs (T cell depleted)	94.6 ± 8.2 (14 weeks)	n.d.	5.8 ± 4.9 (18 weeks) 1.4×10^6 MNCs (T cell depleted)
SU718	BM	APL with *PML–RARA*	1×10^6 MNCs (FACS-sorted blasts)	97.2 ± 1.3 (24 weeks)	n.d.	n.d.
SU748	pB	APL with *PML–RARA*	0.9×10^6 MNCs (FACS-sorted blasts)	78.9 ± 32.3 (24 weeks)	n.d.	n.d.
SU380	pB	AML with inv(16)(p13;q22) or t(16;16)(p13;q22)	0.8×10^6 $CD45^{dim}$ (FACS-sorted blasts)	98.1 ± 0.7 (16 weeks)	n.d.	6.2 ± 3.3 (18 weeks) 1×10^6 MNCs (T cell depleted)
SU080	BM	AML with inv(16)(p13;q22) or t(16;16)(p13;q22)	0.5×10^6 $CD45^{dim}$ (FACS-sorted blasts)	95.7 ± 2.2 (8 weeks)	n.d.	No engraftment (11 weeks) 0.5×10^6 $CD34^+$ blasts (T cell depleted)
SU430	pB	BAL	0.75×10^6 MNCs (T cell depleted)	98.5 ± 2.4 (17 weeks)	n.d.	93.8 ± 7.2 (16 weeks) 1×10^6 MNCs (T cell depleted)
SU028	Leuk	AML n.o.s.	100 MNCs (T cell depleted)	98.6 ± 1.8 (14 weeks)	n.d.	94.8 ± 2.9 (25 weeks) 5×10^6 MNCs (T cell depleted)
SU048	Leuk	AML n.o.s.	1000 MNCs (T-cell depleted)	97.6 ± 3.6 (14 weeks)	n.d.	98.1 ± 1.1 (12–15 weeks) 5×10^6 MNCs (T cell depleted)
SU507	pB	BAL	1×10^6 MNCs (T cell depleted)	Normal engraftment	n.d.	<1% normal engraftment (18 weeks) 1×10^6 MNCs (T cell depleted)
SU421	pB	AML with t(8;21)(q22;q22)	0.13×10^6 $CD45^{dim}$ (FACS-sorted blasts)	No engraftment (13 weeks)	No engraftment (18 weeks)	n.d.

Abbreviations: pB, peripheral blood; BM, bone marrow; n.o.s., not otherwise specified; BAL, biphenotypic acute leukemia; MNCs, mononuclear cells; leuk, leukapheresis; i.o., intraossicle; i.v., intravenous; n.d., not determined. Normal engraftment is defined as multi-lineage engraftment consisting mainly of B cells, with minor percentages of myeloid cells.

was detected in directly injected humanized ossicles, whereas there was almost undetectable engraftment in the BM of unmanipulated NSG mice (mean ± s.d.; 89.6 ± 10.4% versus 2.1 ± 4.6%; $P < 0.0001$) (**Fig. 2b**). Leukemia cells that initially engrafted in humanized ossicles after direct injection preferentially disseminated to nontransplanted ossicles rather than to the BM of the same mouse, over the course of 8–24 weeks after transplantation (mean ± s.d. at 8 weeks, 22.1 ± 26.9% versus 4.6 ± 3.9%; $P = 0.09$; 12–13 weeks, 74.1 ± 30.4% versus 30.37 ± 40.9%; $P < 0.05$; 18–24 weeks, 88.5 ± 17.7% versus 60.8 ± 33.6%; $P < 0.05$ (**Fig. 2b**). Histological analysis 8 weeks after transplantation recapitulated the flow cytometry results, demonstrating high human $CD45^+$ leukemia cell burden in the directly injected ossicles, and it revealed low-level engraftment and repopulation in the nontransplanted ossicles of the same mice (**Fig. 2c**). In the nontransplanted ossicles, human leukemia cells were almost exclusively localized to the endosteal paratrabecular regions that have previously been demonstrated to be preferred niches for both normal HSCs and AML LSCs[15,21].

A similar preferential engraftment of the humanized niches was observed in intravenously injected mice bearing ossicles. At 8 weeks after transplantation, all ossicles were engrafted with human leukemia cells, whereas the mouse BM showed significantly less engraftment, and in some cases, even a complete absence of human cells (mean ± s.d.; 8 weeks, 14.4 ± 19.1% versus 2.5 ± 1.8%; $P < 0.01$) (**Fig. 2a**,**b** and **Supplementary Figs. 3** and **4**). Subsequent analysis performed at 12–13 weeks and 18–24 weeks after transplantation demonstrated a continuous statistically significant increase in engraftment in the ossicles, as compared to the mouse BM, reaching near-complete replacement of mouse hematopoiesis in most ossicles by 12–13 weeks (**Fig. 2b**). By 18–24 weeks, the leukemia cell burden in the BM of mice without humanized ossicles was significantly lower than engraftment in the ossicles after intravenous injection (mean ± s.d.; 18–24 weeks. 13.4 ± 20.1% versus 89.5 ± 14.1%; $P < 0.0001$). Notably, the presence of humanized ossicles eventually increased the engraftment of human leukemia in the BM of the same mouse relative to that in unmanipulated mice (mean ± s.d.; 18–24 weeks, 48.0 ± 33.2% versus 13.4 ± 20.1%; $P < 0.001$). As expected, histological analysis demonstrated effacement of the ossicle marrow cavity with human AML cells that showed typical morphological features of myeloid blasts (**Supplementary Fig. 5a**,**b**), and molecular analysis identified leukemia-associated mutations and/or translocations in the engrafted cells (**Supplementary Fig. 5c** and **Supplementary Table 3**).

With these four AML samples, the absolute number of leukemia cells recoverable from humanized ossicle niches in a single mouse (four ossicles per mouse) was significantly higher than the number of cells that could be isolated from the corresponding mouse BM. We recovered an average of $5.8 \pm 1.5 \times 10^7$ (mean ± s.d.; SU306, $5.4 \pm 0.4 \times 10^7$; SU480, $5.2 \pm 0.9 \times 10^7$; SU532, $5.8 \pm 0.1 \times 10^7$; SU582, $5.0 \pm 1.1 \times 10^7$) human leukemia cells, combined from all four explanted ossicles of mice transplanted with samples SU306, SU480, SU532, and SU582. By contrast, absolute leukemia cell counts recoverable from total mouse

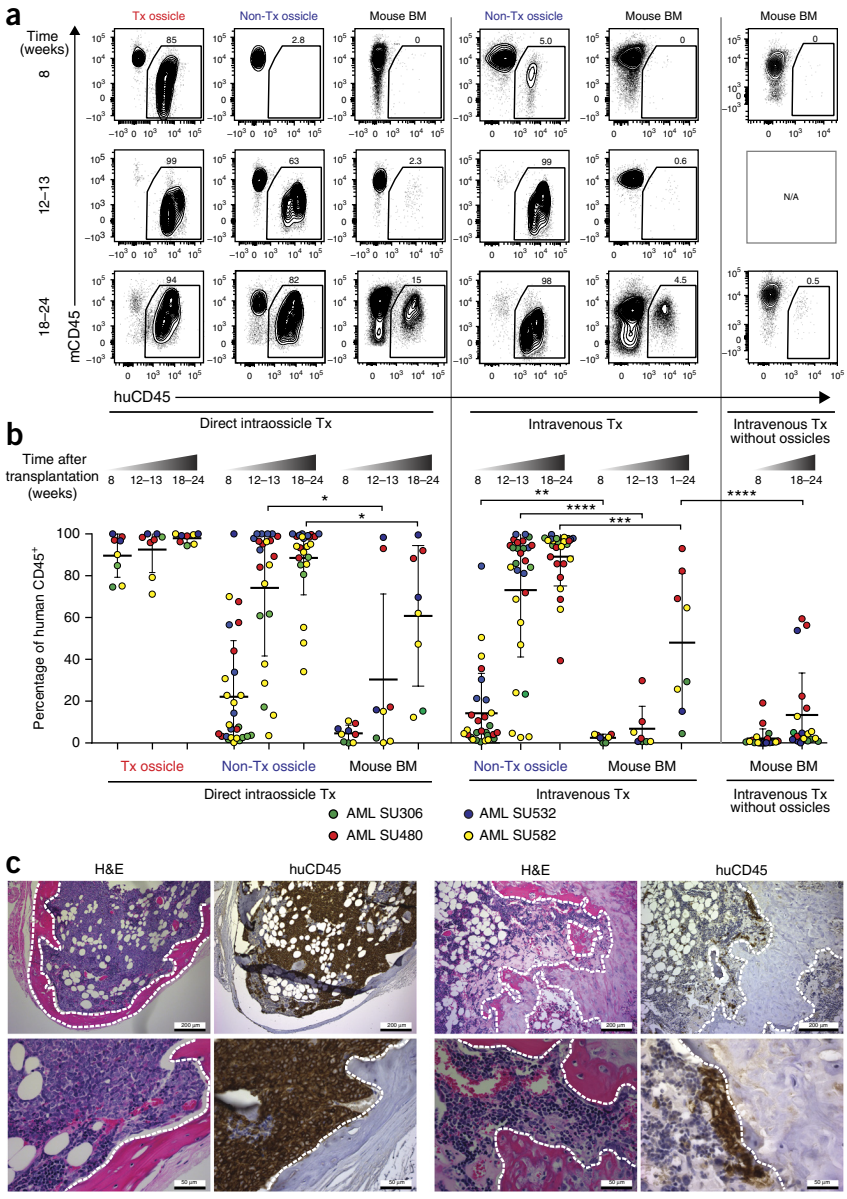

Figure 2 Primary AML blasts preferentially engraft humanized ossicle niches, as compared to mouse BM. (**a**) Representative FACS plots of human leukemia engraftment at 8 weeks, 12–13 weeks, and 18–24 weeks after transplantation. 1×10^6 T cell–depleted mononuclear cells (MNCs) were transplanted (i) directly into one of four humanized ossicle niches per mouse (direct intraossicle Tx); (ii) intravenously into mice bearing four ossicles; or (iii) intravenously into mice without ossicles (left to right). Transplanted (Tx) ossicle and nontransplanted (non-Tx) ossicles, as well as mouse BM, were analyzed for the presence of human $CD45^+CD33^+$ AML cells ($n = 7$–28 per group). (**b**) Summary of human leukemia engraftment over time in the ossicles and mouse BM. Each dot represents one ossicle or mouse BM. Black lines with error bars represent mean engraftment ± s.d. Four different primary AML samples are color coded, as indicated. (Tx ossicle after direct intraossicle Tx, 8 weeks, $n = 8$; 12–13 weeks, $n = 8$; 18–24 weeks, $n = 8$. Non-Tx ossicles after direct intraossicle Tx, 8 weeks, $n = 27$; 12–13 weeks, $n = 22$; 18–24 weeks, $n = 24$. Mouse BM after direct intraossicle Tx, 8 weeks, $n = 9$; 12–13 weeks, $n = 9$; 18–24 weeks, $n = 8$; non-Tx ossicles after intravenous Tx, 8 weeks, $n = 28$; 12–13 weeks, $n = 28$; 18–24 weeks, $n = 28$; mouse BM after intravenous Tx, 8 weeks, $n = 7$; 12–13 weeks, $n = 7$; 18–24 weeks, $n = 7$; mouse BM after intravenous Tx without ossicles, 8 weeks, $n = 12$; 18–24 weeks, $n = 12$) $^*P < 0.05$; $^{**}P < 0.01$; $^{***}P < 0.001$; $^{****}P < 0.0001$, Mann–Whitney U test. (**c**) Representative histological analysis of explanted Tx ossicles (left) and non-Tx ossicles (right) 8 weeks after transplantation. At least two engrafted ossicles were analyzed per primary AML sample SU306, SU480, SU532 and SU582. H&E staining and immunostaining for human CD45 are shown in low (top) and high (bottom) magnification. Scale bars, 200 µm (top) and 50 µm (bottom). White dotted lines indicate endosteal bone surface. N/A, not analyzed.

BM were significantly lower, with an average of $1.6 \pm 2.3 \times 10^7$ human leukemia cells, and varied depending on engraftment level ($P < 0.0001$ for all samples combined, unpaired Student's t test; SU306, $8.9 \pm 1.5 \times 10^6$; SU480, $3.7 \pm 2.7 \times 10^7$; SU532, $1.4 \pm 2.6 \times 10^7$; SU582, $5.9 \pm 4.8 \times 10^6$; **Supplementary Fig. 5d**).

Engrafted cells in humanized ossicles recapitulate the original subclonal architecture

Recent work has suggested that conventional NSG mouse xenograft assays do not fully recapitulate the clonal heterogeneity of patient samples. As a result, engrafting subclones may be distinct from the dominant founding or relapse clones, presumably because of selective pressure imparted by the mouse BM microenvironment[22]. We investigated the clonal composition of human AML cells engrafted in the humanized ossicle niches through targeted re-sequencing of known leukemia mutations in four of the engrafted normal karyotype cases. In all samples analyzed (SU306, SU480, SU532, and SU582), we detected the same variants (SNPs and indels) at similar variant allele frequencies in the primary patient samples and in the ossicle-engrafted leukemia cells at 18–24 weeks after transplantation (**Supplementary Fig. 5c**). Notably, AML blasts transplanted by direct intraossicle injection most closely recapitulated the clonal heterogeneity of the original patient blasts, whereas cells that engrafted in the mouse BM after intravenous transplantation tended to show variable variant allele frequencies (**Supplementary Fig. 5c**, bottom) For example, at sample SU532, a canonical mutation in the *NPM1* gene was detected at similar levels in both the original blasts and the cells from the engrafted ossicles; however, a subclone without this *NPM1* mutation engrafted the mouse BM of animals that received intravenous transplants, demonstrating that engraftment of the original clone occurred only in the ossicle model.

Ossicle transplantation reveals a higher frequency of leukemia-initiating cells

Original studies using limiting-dilution xenograft assays suggested that LICs in AML were rare, comprising 1:10,000 or fewer cells[23,24].

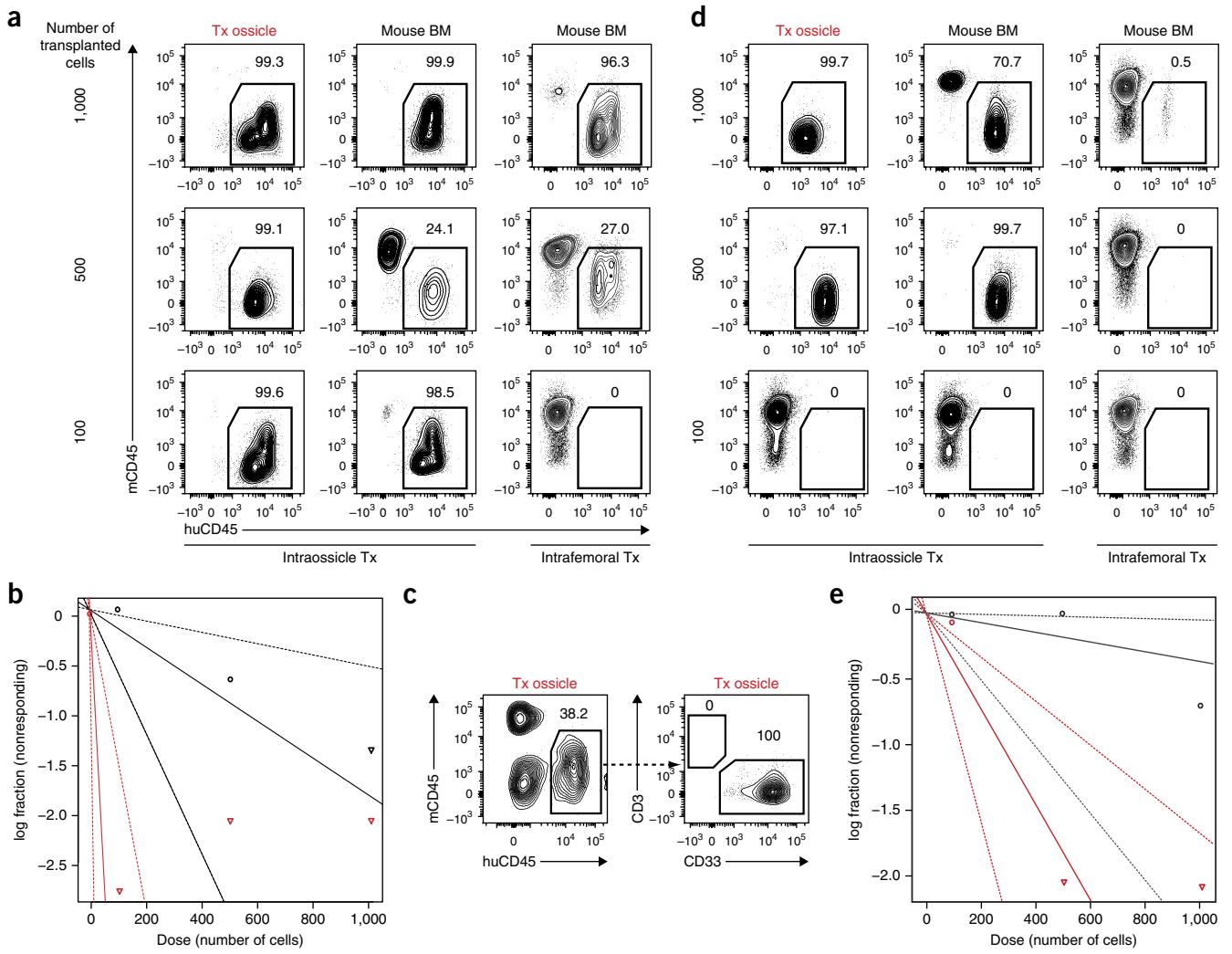

Figure 3 Humanized ossicle niche transplantation reveals an increased LIC frequency in AML. (**a**,**d**) Varying numbers (1,000; 500; 100; 1) of T cell–depleted MNCs from AML samples SU028 (**a**) and SU048 (**d**) were transplanted directly into humanized ossicle niches (intraossicle Tx) or intrafemorally into NSG mice. Engraftment was analyzed 14 weeks after transplantation by flow cytometry. Representative FACS plots ($n = 2$–24 per group) showing human leukemia engraftment in the ossicles (Tx ossicle), and mouse BM are indicated. (**b**,**e**) The frequency of LICs was determined by limiting-dilution analysis, as described in Methods. A log-fraction plot was fitted to the data provided in **Supplementary Table 4**. Solid lines represent estimated LIC frequencies for intraossicle (red) and intrafemoral (black) transplantation. Dotted lines show 95% confidence intervals. Open dots correspond to transplanted-cell doses that led to no engraftment in individual mice per group. Inverted triangles represent transplanted-cell doses with all mice engrafted per group. (**c**) Engraftment analysis from direct intraossicle transplantation of a single $CD34^+CD38^-$ cell from case SU028 through the monitoring of human $CD45^+CD33^+$ cells in the transplanted ossicle 12 weeks after transplantation.

To determine whether transplantation of AML cells into a humanized microenvironment, relative to unmanipulated NSG mice, reveals a higher frequency of LICs, we conducted limiting-dilution assays with two AML samples using both direct intraossicle transplantation and direct intrafemoral transplantation in unmanipulated NSG mice. Cells from case SU028 demonstrated engraftment in the ossicles in all mice transplanted with as few as 100 cells, whereas no engraftment was detected by intrafemoral transplantation with 100 cells (**Fig. 3a**,**b**). In fact, we observed leukemic engraftment from the transplantation of a single SU028 $CD34^+CD38^-$ leukemic blast in a humanized ossicle (**Fig. 3c**), resulting in an approximately 27-fold increase in the frequency of LICs, to 1:20 cells (**Fig. 3b** and **Supplementary Table 4**). In the case of SU048, complete engraftment (>95%) was detected in the injected ossicles from as few as 500 cells, as compared to very low engraftment (<1%) in mice transplanted intrafemorally with 1,000 cells, which resulted in a tenfold increase in LIC frequency, to 1:271 cells (**Fig. 3d**,**e** and **Supplementary Table 4**).

Engraftment of APL cells in ossicles

Transplantation of human APL cells into immunocompromised mice has so far met with limited success, resulting in low to no detectable engraftment[9,24]. Given that humanized ossicle niches show superior engraftment of non-APL AML samples, we attempted to induce the engraftment of primary human APL cells by direct intraossicle injection. We injected 0.9×10^6–1.4×10^6 mononuclear cells from primary APL samples into humanized ossicles and monitored engraftment over time. As early as 6–8 weeks after transplantation, we detected $CD45^+CD33^+$ leukemia cells in injected ossicles (mean ± s.d.; SU589, 41.2 ± 27.4%; SU490, 21.5 ± 8.2%; SU748, 5.1 ± 7.1%; SU718, 0.3 ± 0.5%) (**Fig. 4a**,**b** and **Supplementary Fig. 6a**–**c**).

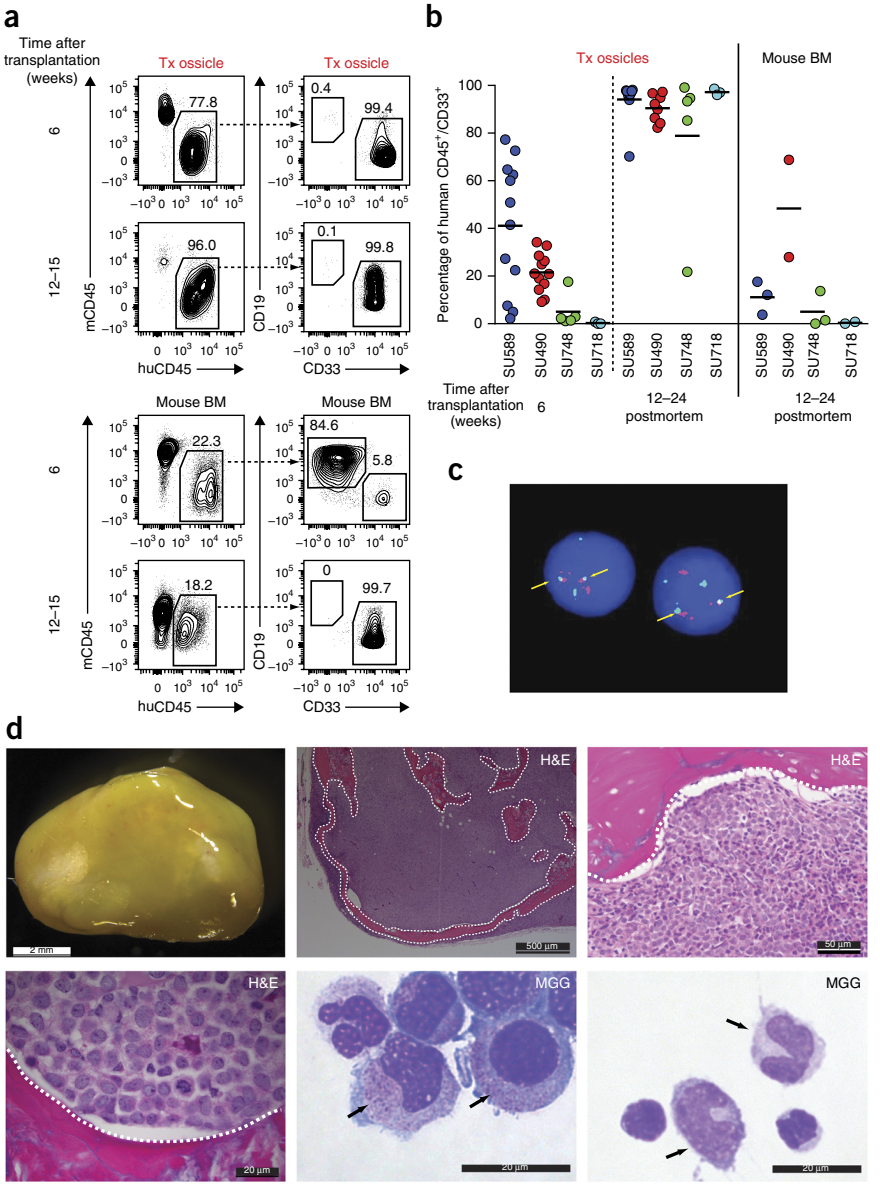

Figure 4 Humanized ossicle niches facilitate robust engraftment of APL cells, which are probably derived from lineage-committed LICs. (**a**) Representative FACS analysis of primary APL cells (sample SU589) showing human CD45$^+$ cells in transplanted ossicles (Tx ossicle, top), as well as mouse BM (bottom), at 6 weeks and 12–15 weeks after transplantation of 1×10^6 primary T cell–depleted MNC ($n = 2$–12 per group) directly into humanized ossicles. The presence of human CD45$^+$CD33$^+$ myeloid cells and CD45$^+$CD19$^+$ lymphoid cells was analyzed. (**b**) Summary of human APL engraftment over time. Each dot represents one transplanted ossicle. Individual APL samples SU589, SU490, SU748, and SU718 are color-coded. Black lines represent mean engraftment (for Tx ossicles, SU589, 6 weeks, $n = 12$; SU490, 6 weeks, $n = 12$; SU748, 6 weeks, $n = 5$; SU718, 6 weeks, $n = 3$; SU589, 12–24 weeks, $n = 12$; SU490, 12–24 weeks, $n = 12$; SU748, 12–24 weeks, $n = 5$; SU718, 12–24 weeks, $n = 3$. For mouse BM, SU589, 12–24 weeks, $n = 3$; SU490, 12–24 weeks, $n = 3$; SU748, 12–24 weeks, $n = 3$; SU718, 12–24 weeks $n = 2$). (**c**) FISH for *PML–RARA* translocation on sorted human CD45$^+$CD33$^+$ blasts from humanized ossicle niches engrafted with primary APL sample SU589. Engrafted APL blasts were FACS-purified as human CD45$^+$CD33$^+$ cells. Yellow arrows mark chromosomal fusion events indicative for t(15;17). Magnification, 100× objective. (**d**) Macroscopic image (top-left) of APL engrafted, explanted humanized ossicle. Scale bar, 2 mm. Histological analysis of explanted engrafted ossicles (H&E, top-middle, top-right, bottom-left) and morphological analysis of engrafted cells on MGG-stained cytospins (bottom-middle and bottom-right). White dashed lines mark the endosteal surface. Black arrows mark azurophilic granules (bottom-middle) and pathognomonic, bilobed, cerebriform APL blasts (bottom right). Scale bars (left to right), 500, 20, 50, and 20 µm.

In two of four samples (SU490 and SU589), although the transplanted cells initially gave rise to both lymphoid and myeloid cells, indicative of normal hematopoietic engraftment, at 6 weeks after transplantation, the eventual outgrowth and proliferation of APL blasts resulted in an almost complete engraftment of the ossicle with leukemia cells at 12–24 weeks (mean ± s.d.; SU589, 94.1 ± 8.5%; SU490, 90.5 ± 5.6%; SU748, 78.9 ± 32.3%; SU718, 97.2 ± 1.3%) (**Fig. 4a**,**b** and **Supplementary Fig. 6a**–**c**), but much lower engraftment of leukemic cells was detected in the mouse BM (**Fig. 4a**,**b**). As shown by fluorescence *in situ* hybridization (FISH), myeloid cells isolated from the engrafted ossicles harbored the human promyelocytic leukemia–retinoic acid receptor-α (*PML–RARA*) oncogene translocation that is characteristic of APL (**Fig. 4c** and **Supplementary Fig. 6a**–**c**). Gross examination of the explanted ossicles revealed the formation of subcutaneous granulocytic sarcomas or chloromas, as indicated by their yellow-green appearance, and histological analysis of engrafted ossicles identified densely packed immature blasts morphologically resembling promyelocytes (**Fig. 4d**). May–Gruenwald–Giemsa (MGG) staining confirmed the presence of azurophilic granules or characteristic cerebriform, bilobed nuclei pathognomonic for the microgranular variant of APL (**Fig. 4d**).

The successful engraftment of primary human APL cells provided us with the opportunity to investigate the immunophenotypic identity of LICs in this disease, which has been a point of controversy in the field[25]. First, we isolated a CD34$^+$CD38$^-$CD45RA$^-$ fraction (containing HSCs and MPPs in healthy BM) from primary APL samples, and we injected these cells or bulk APL cells directly into humanized ossicles. In contrast to bulk cells that transiently (6–8 weeks after transplantation) gave rise to lymphoid and myeloid cells, before being replaced by 100% myeloid cells harboring the *PML–RARA* translocation (**Fig. 4a**), transplanted HSC and MPP produced normal B cells and myeloid cells that lacked the *PML–RARA* translocation for up to 24 weeks (**Supplementary Fig. 6d**,**e**), which suggests that LIC activity in APL resides in a cell that is downstream of the HSC and MPP stage. This idea was further supported by FISH analysis of subpopulations that were isolated from several primary APL samples, which demonstrated that HSCs, MPPs, CMPs, and MEPs lacked the *PML–RARA* translocation in all samples analyzed (**Supplementary Table 5**).

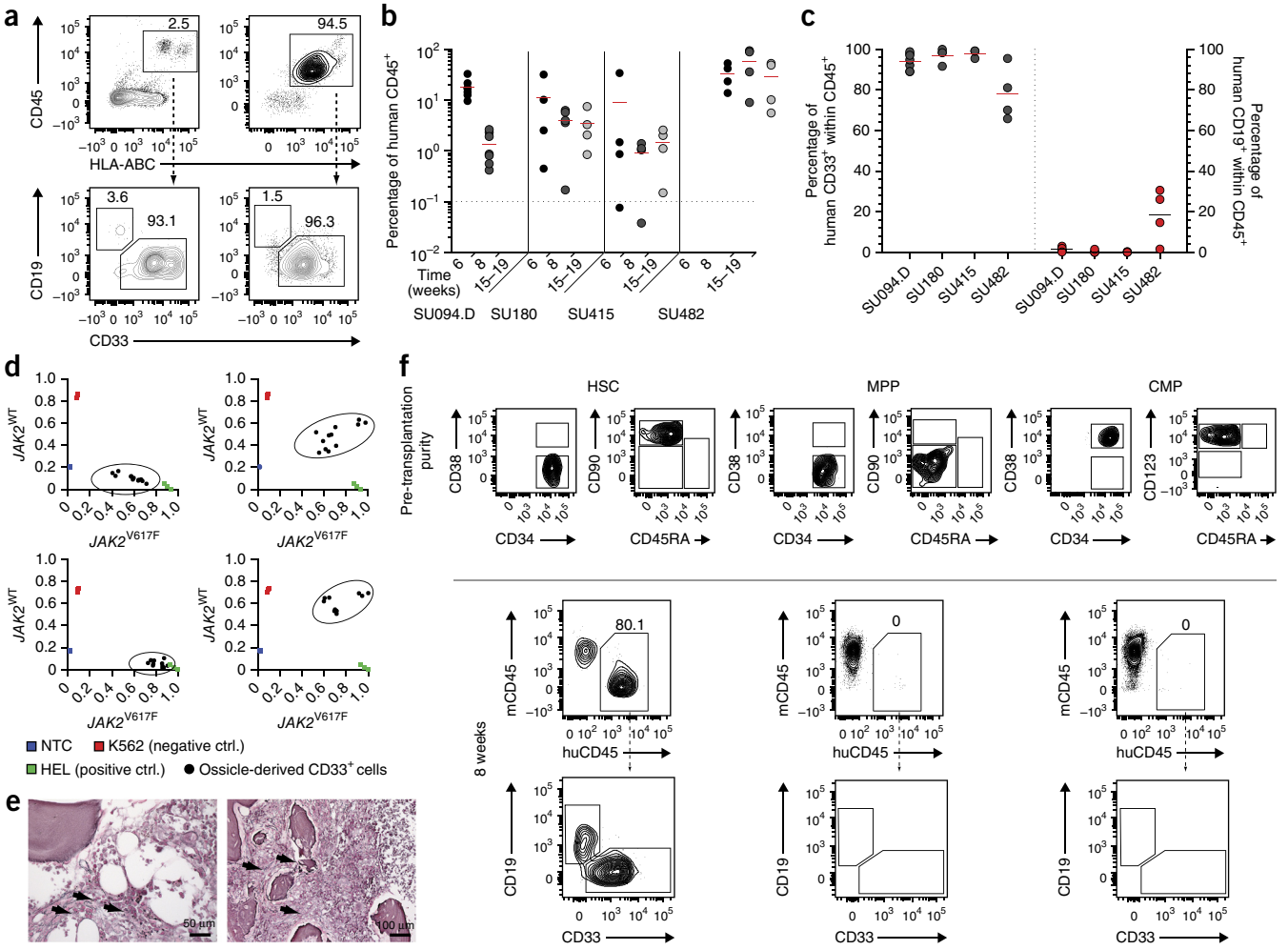

Figure 5 Humanized ossicle niches facilitate robust engraftment of MF, which derives from LICs in the HSC compartment. (**a**) Representative FACS plots showing engraftment 8 weeks after direct intraossicle transplantation of FACS-purified CD34$^+$CD38$^-$ cells from MF samples SU094.D (left) and SU482 (right) (n = 4–7 per sample). (**b**,**c**) Summary of human CD45$^+$ engraftment kinetics (**b**) and the percentage of CD33$^+$ myeloid cells (**c**, gray circles) versus CD19$^+$ B cells (red circles) among engrafted human CD45$^+$ cells at 6 weeks after transplantation of MF samples SU094, SU180, SU415 and SU482. Each dot represents one transplanted ossicle, and horizontal lines indicate mean engraftment levels (SU094.D, n = 7; SU180, n = 4; SU415.D, n = 4; SU482, n = 4). (**d**) *JAK2* mutation status of engrafted CD33$^+$ myeloid cells tested from MF samples SU094.D, SU180 (top), SU451 and SU482 (bottom) by custom Taqman SNP genotyping assays. Cells isolated from ossicles (black ovals) were either classified as wild type (WT) (*JAK2*^{WT}, y axis) or mutated (*JAK2*^{V617F}, x axis), according to comparison with cell lines known to be either WT (K562, red rectangles) or mutated (HEL, green rectangles), or to no template control (NTC, blue rectangles). Reactions were performed in triplicate. (**e**) Reticulin stain of explanted ossicles engrafted with MF sample SU180. Black arrows indicate presence of reticulin fibers. Scale bars, 50 µm (left) and 100 µm (right). (**f**) FACS plots depicting pre-transplantation purity (top) of FACS-purified HSCs, MPPs, and CMPs isolated from MF sample SU482, and the percentage of human CD45$^+$ cell engraftment within transplanted ossicles 8 weeks after transplantation (bottom), and further gated for myeloid cells (CD45$^+$CD33$^+$) and B lymphoid cells (CD45$^+$CD19$^+$).

However, this translocation was detected in aberrant CD34$^{lo/-}$ GMP-like cells, which did give rise to *PML–RARA*-positive APL in transplanted ossicles (**Supplementary Fig. 6e**). Thus, LICs in APL do not reside in HSCs or MPPs, and probably reside in a lineage-committed progenitor.

Ossicles facilitate engraftment of myelofibrosis

Myelofibrosis (MF), an MPN that is commonly associated with the V617F mutation in Janus kinase 2 (*JAK2*^{V617F}) and with calreticulin (*CALR*) mutations[26–29], has shown only limited engraftment in conventional xenograft models[30–32]. We examined the ability of humanized ossicles to facilitate the engraftment of MF (**Supplementary Table 6** for patient sample information) by directly injecting FACS-purified CD34$^+$ cells from patient samples into ossicles. Transplantation of as few as 50,000 CD34$^+$ cells resulted in robust engraftment (up to >95%) of human hematopoietic cells for up to 19 weeks after transplantation (**Fig. 5a**,**b**). Notably, the engrafted cell population consisted mainly of CD33$^+$ myeloid cells, with minimal to absent reconstitution of B cells, which are the predominant population in mice engrafted with healthy human CD34$^+$ cells (**Fig. 5c** and **Supplementary Fig. 2b** for healthy human CD34$^+$ cells). Allele-specific quantitative real-time PCR demonstrated that engrafted human CD45$^+$CD33$^+$ myeloid cells at 8–19 weeks after transplantation harbored the *JAK2*^{V617} mutation in four of four samples, indicating that they were derived from the transplanted MF cells (**Fig. 5d**). The *JAK2*^{V617F} mutated allele burden in the engrafted cells was nearly identical to the allele burden in the HSPCs and myeloid cells isolated from the primary sample in both homozygous (SU094.D, SU415) and heterozygous (SU180,

SU482) scenarios (**Supplementary Fig. 7a**). For sample SU239B cells harboring a type 1 *CALR* mutation (52-bp deletion), we confirmed the presence of the mutation in the engrafted myeloid cells by Sanger sequencing (**Supplementary Fig. 7d**). Consistently with the engraftment of MF-initiating cells, histological analysis identified an increase in reticulin fibers within the engrafted humanized ossicles (**Fig. 5e**).

The successful engraftment of primary human MF cells provided the opportunity to investigate LICs in this disease; these cells have long been hypothesized to reside in the HSC compartment[33]. We first fractionated $CD34^+$ cells from MF samples into $CD34^+CD38^+$ and $CD34^+CD38^{lo/-}$ subfractions and transplanted each directly into multiple humanized ossicles ($n = 4–7$ per sample). In all three samples tested, the engraftment of human cells was observed exclusively in ossicles transplanted with $CD34^+CD38^{-/lo}$ cells ($n = 19$ ossicles), showing no engraftment of $CD34^+CD38^+$ cells ($n = 12$ ossicles), despite the fact that higher numbers of these cells were transplanted (**Supplementary Table 7**). We further fractionated the $CD34^+CD38^{low/-}$ cells from sample SU482 and SU239.B into HSCs and MPPs[34], and tested their engraftment potential through direct intraossicle injection. As a negative control, we also transplanted CMPs from the $CD34^+CD38^+$ fraction (**Supplementary Table 5**). 8 weeks after transplantation, human $CD45^+$ cells were detectable only in ossicles transplanted with HSCs, not with MPPs or CMPs (**Fig. 5f** and **Supplementary Fig. 7b**), and the engrafted myeloid cells harbored the $JAK2^{V617F}$ mutation or the type 1 *CALR* mutation (52-bp deletion) (**Supplementary Fig. 7c,d**). These results formally demonstrate that MF-initiating cells reside exclusively in the HSC compartment.

DISCUSSION

Here we demonstrate that a xenotransplantation system based on the *in situ* subcutaneous generation of human BM-MSC-derived ossicles and the formation of a humanized BM microenvironment supports normal and malignant hematopoiesis more effectively than existing xenotransplantation models. Previous xenotransplantation studies suggested that AML LICs are enriched in the $CD34^+CD38^-$ fraction of leukemic blasts and are rare cells, occurring at a frequency on the order of 1:10,000 to 1:100,000 (refs. 23,24). More recent studies suggest that LICs are more frequent, and that they can be found in additional immunophenotypically defined subpopulations[7,35,36]. Here we provide evidence that the frequency of LICs is substantially higher if evaluated by xenotransplantation into a humanized niche, as compared to the BM of naïve NSG mice, which suggests that the LIC frequency in AML is crucially dependent on leukemia cell–niche interactions.

The identification of disease-initiating cells in APL has been hampered by the lack of a xenotransplantation model. In APL, the nature of the hematopoietic cell that is the target of the disease-causing chromosomal translocation is a matter of debate[25]: *in vitro* studies have implicated immature compartments that are able to produce myeloid and erythroid output[37], whereas other reports support the concept that APL arises from committed myeloid progenitors[38–40]. Here we report successful fulminant engraftment of *PML–RARA*-positive human APL cells in humanized ossicles, and the identification of APL-initiating cells in an aberrant $CD34^{-/lo}$ GMP-like population. This further supports the notion that APL is a disease that arises from committed myeloid cells and that probably does not involve immature HSPCs. Our experiments still leave open the possibility that $CD34^-$ cells, which are the majority of cells in most APL cases, also contain disease-initiating cells. These results are consistent with mouse models that drive the expression of PML–RAR-α from a myeloid lineage–restricted promoter, resulting in an APL-like disease[41,42]. The absence of the *PML–RARA* translocation in human HSCs obtained from APL patient samples is surprising, given that PML–RAR-α on its own induces myeloid commitment, rather than self-renewal, in hematopoietic progenitors such as GMPs[43]. In contrast to a recently published report[44] demonstrating the establishment of APL from transduced cord-blood-derived CMPs, we did not identify *PML–RARA* fusion events in FACS-purified CMPs from primary patient samples. How PML–RAR-α initiates a self-renewal program in human progenitors to cause APL is an important question for further studies of APL pathogenesis.

Our humanized ossicle model, similarly to APL, facilitates robust engraftment of primary human MF cells, which has only been of limited success with peripheral blood cells in conventional NSG models[32,45]. Unlike studies of AML, where disease-initiating cells arise from progenitors[36], we show here that MF-initiating cells reside in the HSC compartment, because transplantation of these cells—but not of MPPs or CMPs—results in the engraftment of $JAK2^{V617F}$ or *CALR*-mutated cells. Notably, the progeny of MF HSCs exhibited a pronounced skewing toward the myeloid lineage, which suggests that the $JAK2^{V617F}$ and *CALR* mutations drive a differentiation program that blocks lymphoid development in favor of myeloid cells.

Recently, several newly developed xenotransplantation models have been reported for improved engraftment of human hematopoietic cells, including modified NSG strains with overexpression or knock-in of human cytokines[2,4,5,46,47], co-transplantation of hematopoietic cells with mesenchymal stromal cells[13], or transplantation of engineered bioscaffolds designed to resemble human BM niches[48]. Although each of these approaches has advantages over conventional NSG mouse models, none has demonstrated the rapid and high leukemic engraftment observed with our humanized ossicle niche model, in which direct intraossicle injection resulted in >95% leukemic chimerism in nearly all engrafting leukemia samples tested. These observations suggest that our approach more faithfully models human disease and provides a superior system for further investigation into human leukemia pathogenesis, leukemia cell–niche interactions, and response to therapeutics.

METHODS

Methods and any associated references are available in the online version of the paper.

Note: Any Supplementary Information and Source Data files are available in the online version of the paper.

ACKNOWLEDGMENTS

We acknowledge the Hematology Division Tissue Bank and the patients for donating their samples. We acknowledge F. Zhao for lab management; N. Hofmann and B. Luo for technical assistance with ossicle analysis and calreticulin sequencing; and the Stanford Cytogenetics Lab for FISH analysis. A.R. is supported by an Erwin-Schroedinger Research Fellowship (Austrian Science Fund) and D.T. by a CJ Martin Overseas Biomedical Research Fellowship (NHMRC, Australia). R.M. is a New York Stem Cell Foundation Robertson Investigator. This research was supported by the New York Stem Cell Foundation and National Institutes of Health grants R01CA188055 and U01HL099999 to R.M. and by funding from the European Union's Horizon 2020 research and innovation programme under grant agreement No. 668724 to D.S.

AUTHOR CONTRIBUTIONS

A.R. and R.M conceived and designed the project. A.R., D.T., M.R.C., W.-J.H., and X.Z. performed the experimental work. A.R., D.T., M.R.C., and D.G. analyzed the data. K.S. and D.S. provided crucial reagents. A.R. and R.M. wrote the manuscript. All authors discussed the results.

COMPETING FINANCIAL INTERESTS
The authors declare no competing financial interests.

1. Doulatov, S., Notta, F., Laurenti, E. & Dick, J.E. Hematopoiesis: a human perspective. *Cell Stem Cell* **10**, 120–136 (2012).
2. Wunderlich, M. *et al.* AML xenograft efficiency is significantly improved in NOD/SCID-IL2RG mice constitutively expressing human SCF, GM-CSF and IL-3. *Leukemia* **24**, 1785–1788 (2010).
3. Nicolini, F.E., Cashman, J.D., Hogge, D.E., Humphries, R.K. & Eaves, C.J. NOD/SCID mice engineered to express human IL-3, GM-CSF and Steel factor constitutively mobilize engrafted human progenitors and compromise human stem cell regeneration. *Leukemia* **18**, 341–347 (2004).
4. Rongvaux, A. *et al.* Development and function of human innate immune cells in a humanized mouse model. *Nat. Biotechnol.* **32**, 364–372 (2014).
5. Willinger, T. *et al.* Human IL-3/GM-CSF knock-in mice support human alveolar macrophage development and human immune responses in the lung. *Proc. Natl. Acad. Sci. USA* **108**, 2390–2395 (2011).
6. Goyama, S., Wunderlich, M. & Mulloy, J.C. Xenograft models for normal and malignant stem cells. *Blood* **125**, 2630–2640 (2015).
7. Sarry, J.E. *et al.* Human acute myelogenous leukemia stem cells are rare and heterogeneous when assayed in NOD/SCID/IL2Rγc-deficient mice. *J. Clin. Invest.* **121**, 384–395 (2011).
8. Sanchez, P.V. *et al.* A robust xenotransplantation model for acute myeloid leukemia. *Leukemia* **23**, 2109–2117 (2009).
9. Patel, S. *et al.* Successful xenografts of AML3 samples in immunodeficient NOD/shi-SCID IL2Rγ$^{-/-}$ mice. *Leukemia* **26**, 2432–2435 (2012).
10. Kim, D., Park, C.Y., Medeiros, B.C. & Weissman, I.L. CD19-CD45$^{low/-}$ CD38$^{high/}$CD138^{+} plasma cells enrich for human tumorigenic myeloma cells. *Leukemia* **26**, 2530–2537 (2012).
11. Kim, D. *et al.* Anti-CD47 antibodies promote phagocytosis and inhibit the growth of human myeloma cells. *Leukemia* **26**, 2538–2545 (2012).
12. Pang, W.W. *et al.* Hematopoietic stem cell and progenitor cell mechanisms in myelodysplastic syndromes. *Proc. Natl. Acad. Sci. USA* **110**, 3011–3016 (2013).
13. Medyouf, H. *et al.* Myelodysplastic cells in patients reprogram mesenchymal stromal cells to establish a transplantable stem cell niche disease unit. *Cell Stem Cell* **14**, 824–837 (2014).
14. Mendelson, A. & Frenette, P.S. Hematopoietic stem cell niche maintenance during homeostasis and regeneration. *Nat. Med.* **20**, 833–846 (2014).
15. Ishikawa, F. *et al.* Chemotherapy-resistant human AML stem cells home to and engraft within the bone-marrow endosteal region. *Nat. Biotechnol.* **25**, 1315–1321 (2007).
16. Schepers, K., Campbell, T.B. & Passegué, E. Normal and leukemic stem cell niches: insights and therapeutic opportunities. *Cell Stem Cell* **16**, 254–267 (2015).
17. Reinisch, A. *et al.* Epigenetic and *in vivo* comparison of diverse MSC sources reveals an endochondral signature for human hematopoietic niche formation. *Blood* **125**, 249–260 (2015).
18. Saito, Y. *et al.* Identification of therapeutic targets for quiescent, chemotherapy-resistant human leukemia stem cells. *Sci. Transl. Med.* **2**, 17ra9 (2010).
19. Song, J. *et al.* An *in vivo* model to study and manipulate the hematopoietic stem cell niche. *Blood* **115**, 2592–2600 (2010).
20. Pettway, G.J. *et al.* Anabolic actions of PTH (1-34): use of a novel tissue engineering model to investigate temporal effects on bone. *Bone* **36**, 959–970 (2005).
21. Zhang, J. *et al.* Identification of the haematopoietic stem cell niche and control of the niche size. *Nature* **425**, 836–841 (2003).
22. Klco, J.M. *et al.* Functional heterogeneity of genetically defined subclones in acute myeloid leukemia. *Cancer Cell* **25**, 379–392 (2014).
23. Lapidot, T. *et al.* A cell initiating human acute myeloid leukaemia after transplantation into SCID mice. *Nature* **367**, 645–648 (1994).
24. Bonnet, D. & Dick, J.E. Human acute myeloid leukemia is organized as a hierarchy that originates from a primitive hematopoietic cell. *Nat. Med.* **3**, 730–737 (1997).
25. Grimwade, D. & Enver, T. Acute promyelocytic leukemia: where does it stem from? *Leukemia* **18**, 375–384 (2004).
26. Kralovics, R. *et al.* A gain-of-function mutation of *JAK2* in myeloproliferative disorders. *N. Engl. J. Med.* **352**, 1779–1790 (2005).
27. Baxter, E.J. *et al.* Cancer Genome Project. Acquired mutation of the tyrosine kinase *JAK2* in human myeloproliferative disorders. *Lancet* **365**, 1054–1061 (2005).
28. Klampfl, T. *et al.* Somatic mutations of calreticulin in myeloproliferative neoplasms. *N. Engl. J. Med.* **369**, 2379–2390 (2013).
29. Nangalia, J. *et al.* Somatic *CALR* mutations in myeloproliferative neoplasms with nonmutated *JAK2*. *N. Engl. J. Med.* **369**, 2391–2405 (2013).
30. James, C. *et al.* The hematopoietic stem cell compartment of *JAK2*^{V617F}-positive myeloproliferative disorders is a reflection of disease heterogeneity. *Blood* **112**, 2429–2438 (2008).
31. Ishii, T. *et al.* Behavior of CD34^{+} cells isolated from patients with polycythemia vera in NOD/SCID mice. *Exp. Hematol.* **35**, 1633–1640 (2007).
32. Wang, X. *et al.* Spleens of myelofibrosis patients contain malignant hematopoietic stem cells. *J. Clin. Invest.* **122**, 3888–3899 (2012).
33. Dameshek, W. Some speculations on the myeloproliferative syndromes. *Blood* **6**, 372–375 (1951).
34. Majeti, R., Park, C.Y. & Weissman, I.L. Identification of a hierarchy of multipotent hematopoietic progenitors in human cord blood. *Cell Stem Cell* **1**, 635–645 (2007).
35. Eppert, K. *et al.* Stem cell gene expression programs influence clinical outcome in human leukemia. *Nat. Med.* **17**, 1086–1093 (2011).
36. Goardon, N. *et al.* Coexistence of LMPP-like and GMP-like leukemia stem cells in acute myeloid leukemia. *Cancer Cell* **19**, 138–152 (2011).
37. Takatsuki, H. *et al.* PML/RARα fusion gene is expressed in both granuloid/macrophage and erythroid colonies in acute promyelocytic leukaemia. *Br. J. Haematol.* **85**, 477–482 (1993).
38. Turhan, A.G. *et al.* Highly purified primitive hematopoietic stem cells are PML-RARA negative and generate nonclonal progenitors in acute promyelocytic leukemia. *Blood* **85**, 2154–2161 (1995).
39. Haferlach, T. *et al.* Cell lineage specific involvement in acute promyelocytic leukaemia (APL) using a combination of May-Grünwald-Giemsa staining and fluorescence in situ hybridization techniques for the detection of the translocation t(15;17)(q22;q12). *Br. J. Haematol.* **103**, 93–99 (1998).
40. Knuutila, S. *et al.* Cell lineage involvement of recurrent chromosomal abnormalities in hematologic neoplasms. *Genes Chromosom. Cancer* **10**, 95–102 (1994).
41. Guibal, F.C. *et al.* Identification of a myeloid committed progenitor as the cancer-initiating cell in acute promyelocytic leukemia. *Blood* **114**, 5415–5425 (2009).
42. Brown, D. *et al.* A PMLRARα transgene initiates murine acute promyelocytic leukemia. *Proc. Natl. Acad. Sci. USA* **94**, 2551–2556 (1997).
43. Grignani, F. *et al.* PML/RAR alpha fusion protein expression in normal human hematopoietic progenitors dictates myeloid commitment and the promyelocytic phenotype. *Blood* **96**, 1531–1537 (2000).
44. Matsushita, H. *et al.* Establishment of a humanized APL model via the transplantation of PML-RARA-transduced human common myeloid progenitors into immunodeficient mice. *PLoS One* **9**, e111082 (2014).
45. Wang, X. *et al.* Sequential treatment of CD34^{+} cells from patients with primary myelofibrosis with chromatin-modifying agents eliminate JAK2^{V617F}-positive NOD/SCID marrow repopulating cells. *Blood* **116**, 5972–5982 (2010).
46. Rongvaux, A. *et al.* Human thrombopoietin knockin mice efficiently support human hematopoiesis *in vivo*. *Proc. Natl. Acad. Sci. USA* **108**, 2378–2383 (2011).
47. Willinger, T., Rongvaux, A., Strowig, T., Manz, M.G. & Flavell, R.A. Improving human hemato-lymphoid-system mice by cytokine knock-in gene replacement. *Trends Immunol.* **32**, 321–327 (2011).
48. Groen, R.W. *et al.* Reconstructing the human hematopoietic niche in immunodeficient mice: opportunities for studying primary multiple myeloma. *Blood* **120**, e9–e16 (2012).

ONLINE METHODS

Primary human samples. AML, ALL, MF, and cord-blood samples were obtained according to the Administrative Panel on Human Subjects Research Institutional Review Board (IRB)-approved protocols (Stanford IRB no. 18329, no. 6453, and no. 5637) with informed consent. Cord blood was collected with written informed consent from the mother, which was obtained before delivery of full-term pregnancies at the Lucile Packard Children's Hospital, according to IRB-approved protocols (Stanford IRB no. 5637), or purchased from the New York Blood Center (NYBC). All cord-blood samples were processed within 24 h after delivery and used fresh. All of the primary AML samples used in this study were tested for recurrent somatic mutations, including ones in *FLT3, NPM1, IDH1*, and *IDH2*, by the Stanford Anatomic Pathology and Clinical Laboratories.

Animal care. All mouse experiments were conducted in accordance with a protocol approved by the Institutional Animal Care and Use Committee (Stanford Administrative Panel on Laboratory Animal Care no. 22264) and in adherence with the US National Institutes of Health's Guide for the Care and Use of Laboratory Animals[49].

BM-MSC culture and immunophenotyping. Human BM samples were obtained according to the Medical University of Graz Ethikkommission (IRB-approved protocol, MUG Graz IRB no. 19-252). BM-MSCs were isolated and expanded, as previously described[17,50,51]. Age of healthy BM donors ranged from 21 to 45 years. Briefly, BM-MNCs were washed out from BM-collection filters by flushing the filters with pre-warmed PBS. Total washouts were spun down (300*g*, 7 min, 4 °C) and resuspended in pre-warmed α-modified minimum essential medium (α-MEM; Sigma-Aldrich, St. Louis, MO) containing 10% pooled human platelet lysate (pHPL) and seeded into culture vessels. Nonadherent cells were removed by rinsing the plastic with PBS, and adherent cells were further expanded. Emerging colonies (CFU-F) were passaged for further cell propagation. For large-scale expansions before transplantation into NSG mice, BM-MSCs were cultured in four-layered cell factories (CF-4, Thermo Fisher, Nunc, Pittsburg, PA) with half-weekly medium changes until the cells reached confluence. At the end of passage 1 (p1), BM-MSCs were profiled for the expression of consensus MSC surface markers[52]. Briefly, trypsinized cells were blocked with sheep serum (10% v/v) and, thereafter, stained with the following monoclonal antibodies for 30 min at 4 °C in the dark: CD90-BUV395 (dilution 1:5; clone 5E10), CD73-PE (dilution 1:33; clone AD2), CD29-APC (dilution 1:100; clone MAR4), CD45-APC (dilution 1:25; clone 2D1), CD14-PE (dilution 1:25 clone MφP9), CD34-PE-Cy7 (dilution 1:50; clone 8G12), CD19-BUV395 (dilution 1:25; clone SJ25C1, all BD Biosciences, San Jose, CA), CD105-eF450 (dilution 1:25; clone SN6), HLA-DR-eF450 (dilution 1:50; clone L243, both ebioscience, San Diego, CA) and corresponding isotype controls. At least 10,000 viable cells (FVD eF520; dilution 1:100; ebiosience) were acquired and analyzed using a BD Fortessa flow cytometer. Raw FCS files were analyzed using FlowJo software (Treestar, Ashland, OR), and histograms were generated.

Humanized ossicle niche formation. Confluent BM-MSCs were harvested using trypsin-based dissociation reagent (TrypLE Express, Thermo Fisher, Gibco). 2×10^6 MSCs were pelleted and resuspended in 60 µl of pHPL and admixed with 240 µl of matrigel-equivalent matrix (Angiogenesis Assay Kit, Millipore, Billerica, MA). A total volume of 300 µl of matrix–cell mixtures was injected subcutaneously to generate humanized ossicle niches (up to four injections per mouse) into the flanks of 6–12-week-old immunodeficient NOD.Cg-*Prkdc*^{scid}*Il2rg*^{tm1Wjl}/SzJ (NSG) mice (Jackson Laboratory, Bar Harbor, ME). Starting at day 3–7, mice received daily subcutaneous injections of human parathyroid hormone (PTH (1–34); R&D Systems, Minneapolis, MN; 40 µg/kg body weight; dorsal neck fold) for 28 consecutive days to further promote BM niche formation, as previously described[19,20]. 8–10 weeks after BM-MSC application, the site of injection was shaved, and transplants were evaluated for bone and marrow formation by palpation and by visual inspection (development of a purple hue is indicative of BM niche formation).

NSG hematopoietic xenotransplantation. Untreated female NSG mice (aged 6–8 weeks) or mice with established humanized ossicle niches were conditioned with 200 rad of irradiation 12–24 h before transplantation (Faxitron, X-ray irradiation). Cells were transplanted either (i) intravenously (150 µl into lateral tail vein) into untreated mice; (ii) intravenously into mice bearing four humanized ossicle niches; or (iii) by direct intraossicle injection into one or up to four humanized ossicle niches per mouse (20 µl). For transplantation, two to five mice were randomly assigned to the different groups, as described above.

HSPCs were enriched from freshly processed cord-blood samples by magnetic separation using CD34 microbeads (Miltenyi Biotec, San Diego, CA), according to the manufacturer's instructions. (1×10^4)–(1×10^5) purified CD34$^+$ HSPCs (purity >95%) were transplanted. Freshly thawed primary AML samples were either subjected to T cell depletion using anti-CD3 magnetic beads (Robosep, Stem Cell Technologies, Vancouver, Canada) or FACS-purified (Aria II, BD Biosciences) on the basis of their side-scatter properties and low CD45 expression on AML blasts. (1×10^6)–(5×10^6) T cell–depleted or FACS-purified AML cells were transplanted. Freshly thawed MF samples were FACS-sorted using a previously established panel that included anti-human lineage markers CD2 (clone RPA-2.10), CD3 (clone HIT3a), CD4 (clone RPA-T4), CD7 (clone M-T701), CD8 (clone RPA-T8), CD11b (clone ICRF44), CD14 (clone MφP9), CD16 (clone 3G8), CD19 (clone H1B9), CD20 (clone 2H7), CD56 (clone B159, all PE-Cy5; all dilution 1:50), GPA-PE-Cy5 (dilution 1:100; clone GA-R2, all BD). Additionally, the following antibodies were used: CD38-PE-Cy7 (dilution 1:50; clone HB7), CD90-FITC (dilution 1:25; clone 5E10), CD123-PE (dilution 1:10 clone 7G3), CD34-APC (dilution 1:25; clone 8G12, all BD), CD10-APC-Cy7 (dilution 1:10; clone HI10a), and CD45RA-BV605 (dilution 1:20; clone HI100, both BioLegend, San Diego, CA). Double-sorted, live, propidium-iodide^{neg} (PI, Thermo Fisher; final concentration, 1 µg/ml) HSPC subpopulations (purity >95%) were transplanted. For limiting-dilution analysis, cells were additionally applied intrafemorally through direct injection into the mouse femur (20 µl). For single-cell transplantation, Lin$^-$CD34$^+$CD38$^-$ cells were sorted into single wells of Terasaki plates (Nunc MiniTrays, Thermo Fisher) prefilled with 10 µl of IMDM 10% FBS, as previously described[53], using FACS AriaII. The efficiency of single-cell sorting was evaluated by microscopic inspection of an additional sorted plate. Cells were transferred into 31G insulin needles and transplanted directly into humanized ossicle niches.

For secondary transplantation, 7,500 FACS-purified CD34$^+$ cells isolated from engrafted ossicles were transplanted into irradiated NSG mice with and without pre-established ossicle niches.

Assessment of human engraftment. Engraftment of human cells within humanized BM-niches or mouse BM was assessed in a nonblinded fashion. BM aspirates were taken directly from engrafted humanized niches or the corresponding mouse BM using 27.5G syringes. In some cases, marrow from individual ossicles could not be successfully aspirated because of technical failure. Those ossicles were excluded from the analysis. For postmortem analysis, explanted ossicles were crushed using a mortar and pestle, and mouse BM (femur and tibia) were flushed. To remove contaminating red blood cells, ACK lysis was performed (RBC lysis buffer, ebioscience). Thereafter, cells were blocked for nonspecific-antibody binding (10% vol/vol sheep serum, 20 min, 4 °C) and stained (30 min, 4 °C, dark) with fluorochrome-conjugated monoclonal antibodies binding human CD45-V450 (dilution 1:25; clone HI30), CD19-APC (dilution 1:25; clone HIB19), CD3-APC-Cy7 (dilution 1:50; clone SK7), CD33-PE (dilution 1:25; clone WM53), mouse CD45.1-PE-Cy5 (dilution: 1:100; clone 30-F11, all BD) and HLA-ABC-FITC (dilution 1:50; clone W6/32, ebioscience). Normal multi-lineage engraftment was defined by the presence of myeloid cells (CD33$^+$) and B cells (CD19$^+$) among engrafted human CD45$^+$ HLA-ABC$^+$ cells. AML engraftment was defined by the presence of a CD45$^+$CD33$^+$ population and absence of other hematopoietic cell populations. Mice engrafted with cord blood were additionally stained with antibodies to CD14-PE (dilution 1:100; clone MφP9), CD15-FITC (dilution 1:50; clone MMA), CD117-APC (dilution 1:25; clone YB5.B8), CD11c-V450 (dilution 1:25; clone B-Ly6), CD11b-PE-Cy7 (dilution 1:25; clone ICRF44), CD123-PE (dilution 1:10; clone 7G3), kappa-light chain-FITC (dilution 1:50; clone TB28-2), lambda-light chain-PE (dilution 1:50; clone 1-155-2), CD41-APC (dilution 1:25; clone HIP8) and CD235a-PE (dilution 1:100; clone

doi:10.1038/nm.4103

GA-R2 all BD), HLA-DR-eF450 (dilution 1:25; clone LN3), FcER1-FITC (dilution 1:25; clone AER-37), mCD45-APC-Cy7 (dilution 1:25; clone A20, all ebioscience), CD1c (BDCA-1)-APC (dilution 1:10; clone AD5-8E7), CD303 (BDCA-2)-APC (dilution 1:10; clone AC144, both Miltenyi) and CD56-APC-Cy7 (dilution 1:25; clone 5.1H11, BioLegend) to further assess myeloid, lymphoid, erythroid, and megakaryocyte lineage. In particular, CD41a and CD235a antibodies specifically recognize human but not mouse antigens.

***JAK2* genotyping.** Allele-specific *JAK2* genotyping assays were performed, as described previously[54]. Briefly, engrafted human B cells (huCD45$^+$CD19$^+$) and myeloid cells (huCD45$^+$CD33$^+$) were sorted on an Aria II flow cytometer (BD) for analysis. Genomic DNA was isolated using QIAmp DNA mini kit (Quiagen, Valencia, CA), amplified (14 cycles, using allele specific primers), and thereafter subjected to qPCR using TaqMan SNP genotyping assay (Applied Biosystems, Thermo Fisher) according to the manufacturer's instructions.

***CALR* mutation screening.** Genomic DNA was isolated from FACS sorted CD33$^+$ engrafted myeloid cells, and 150 ng was amplified (25 cycles) using PCR SuperMix High Fidelity (Invitrogen). Forward primer, 5′-TGTAAAACG ACGGCCAGTAAGCAAGGGCTATCGGGTAT-3′; reverse primer, 5′-CAGG AAACAGCTATGACCAACCAAAATCCACCCCAAAT-3′. Final primer concentration was 200 nM, annealing temperature and extension temperature were 56 °C and 68 °C, respectively. PCR products were purified with QIAquick PCR Purification Kit (Qiagen), and Sanger sequencing was performed to determine specific indels. Sequencing primer, 5′-TGTAAAACGACGGCCAGT-3′.

AML sample genotyping. AML samples engrafted in ossicles or corresponding mouse BM, as well as sorted CD45^{dim} AML blasts and CD3$^+$ T cells from patients with AML, were genotyped by customized hybrid capture sequencing (SeqCap EZ Choice kit, Roche/Nimblege, Madison, WI) targeting 130 of the most frequently mutated genes in AML. The native samples (before xenotransplantation) were genotyped by whole-exome sequencing (SeqCap EZ Exome SR kit v3.0, Roche/Nimblegen), as previously described[55]. All kits were used according to the manufacturer's instructions (Roche/Nimblegen). Illumina HiSeq 2000, HiSeq 2500, or NextSeq 500 instruments were used for sequencing.

Morphological analysis. FACS-sorted purified cells were spun onto Poly-L-lysine pre-coated slides (Shandon Cytospin centrifuge, Thermo Electric). MGG staining was performed using standard procedures. Light-microscopy images were taken on a Leica DM5500B microscope equipped with Leica Application Suite V4 software (Leica Microsystems, Buffalo Grove, IL).

Fluorescence *in situ* hybridization. Engrafted FACS-purified myeloid cells were FACS-sorted, treated with hypotonic solution (0.075 M KCl, 15 min, 37 °C) and fixed with methanol and glacial acid (3: 1, 30 min, RT) before spinning onto Poly-L-lysine pre-coated slides. Interphase FISH analysis for t(15;17) or inv16 was performed using a PML–RARA Dual Color, Dual Fusion Translocation Probe or CBFB break apart Probe (Abbott, Des Plaines, IL), Briefly, ethanol-dehydrated specimens, pretreated per the manufacturer's instructions, were denatured (80 °C, 8 min) and hybridized (37 °C, 20 h) using a VysisHYBrite instrument. Slides were washed with 0.4× saline sodium citrate (SSC) (0.3% NP-40, pH 7.0, 73 °C, 2 min) and with 2× SSC (pH 7.0, RT, 2 min) counterstained with DAPI and analyzed on an Olympus BX51 microscope equipped with an 100× oil-immersion objective, appropriate fluorescence filters, and CytoVision imaging software (Leica Microsystems). Whenever possible, 200 nuclei were analyzed per condition.

Histological studies. *Immunohistochemistry (IHC).* Tissues were fixed with 4% paraformaldehyde immediately after explantation. H&E staining and IHC staining were performed using standard protocols[17]. For IHC staining, temperature-based antigen retrieval was performed (70 °C, 160 W, 40 min), followed by a descending alcohol series. Endogenous peroxidases were blocked with hydrogen peroxide (10 min) and nonspecific-antibody binding with Ultra V Block (5 min; Thermo Fisher), followed by mouse-on-mouse blocking (MOM, 1 h; Vector Laboratories, Burlingame, CA) and serum-free protein block (30 min; Dako, Glostrup, Denmark). Slides were incubated (30 min, RT) with unconjugated monoclonal mouse anti-human antibodies against CD45 (dilution 1:1,000; clone 2B11, Dako) and developed with ultravision LP large volume detection system horseradish peroxidase (HRP) polymer (Thermo Fisher) and diaminobenzidine (DAB) according to the manufacturer's instructions. Cells were counterstained (10 s) with hematoxylin.

Reticulin staining. Tissue sections were deparaffinized and rehydrated with distilled water. Slides were oxidized in 0.5% potassium permanganate (5 min) before being rinsed in running tap water (2 min). 2% potassium metabisulfite was applied (2 min), and samples were again rinsed in running tap water (2 min) and then sensitized in 2% ferric ammonium sulfate (10 min). After another rigorous rinse in distilled water (1 min), ammoniacal silver nitrate solution was applied (5 min) and thereafter rinsed quickly in three changes of distilled water (30 s each). Slides were transferred to 20% unbuffered formalin rinsed in running tap water (2 min) and toned in 0.2% gold chloride (10 min). Another rinse in running tap water for 1 min was followed by incubation with 2% potassium metabisulfite (2 min). After rinsing in running tap water (1 min), excess silver in 2% sodium thiosulfate was removed (2 min). Eventually, slides were dehydrated, cleared, and mounted with a coverslip. For the detection of GFP$^+$ MSC-derived cells, explanted ossicles were fixed in 2% PFA at 4 °C overnight, and then decalcified (Decal Solution, American Mastertech, Lodi, CA) for 2–8 h. Specimens were processed for embedding in OCT by cryoprotection in sucrose and sectioned on a cryotome. Representative sections were counterstained with DAPI, and thereafter, a standard H&E staining was performed. All images were captured using a Leica DM5500 microscope and Leica Application Suite V4 software.

Lentiviral production. HEK293TN cells (System Biosciences, Mountain View, CA) were grown in DMEM high-glucose medium (Hyclone, GE Healthcare Life Sciences, Pittsburgh, PA)) supplemented with 10% FBS, 2 mM poly-L-glutamine, 25 mM HEPES, and 1× nonessential amino acids (NEAA, Thermo). 24 h before transfection, 8×10^6–9×10^6 cells were plated in a 150-mm tissue-culture dish. For transfection, 13.5 µg of the GIPZ lentiviral shRNA plasmid expressing a scrambled RNA control was combined with 8.8 µg of the packaging vector psPAX2 and 4.7 µg of the envelope-expressing plasmid pCMV-VSV-G. The DNA mixture was diluted in Opti-MEM I medium (Thermo Fisher) and admixed with 293fectin transfection reagent (Thermo Fisher) at a ratio of 3 µl per 1 µg of DNA and, thereafter, dropwise added to HEK293TN cells. Viral supernatant was collected at 60 h after transfection, filtered through a 0.45 µm PVDF filter and concentrated through ultracentrifugation (Sorvall, Thermo Fisher; 23,000 rpm, 4 °C, 2 h). The concentrated lentiviral particles were resuspended overnight in HBSS with 25 mM HEPES and stored at −80 °C.

Lentiviral transduction. Early passage BM-MSCs were cultured in 10-cm dishes to 70–80% confluence in α-MEM supplemented with 10% pHPL. For transduction α-MEM was removed, cells were washed twice with pre-warmed PBS and lentiviral particles were added in 5 ml OptiMEM I medium supplemented with 2% FBS and 50 µg/ml protamine sulfate (Sigma-Aldrich). Lentiviral particles were removed after 8 h, and cells were changed back to standard α-MEM 10% pHPL. After 2 d of recovery, transduced cells were selected by adding 5 µg/ml puromycin for 48 h. GFP$^+$ cells were passaged and further expanded to reach quantities sufficient for transplantation for humanized ossicle niche formation.

Absolute quantification of engrafted leukemia cells. The total number of mCD45.1$^+$ nucleated cells recoverable per humanized ossicle niche or mouse femur was quantified using Countbright absolute counting beads (Thermo Fisher) on a FACS Canto II flow cytometer (BD). The absolute number of total mouse BM cells was extrapolated, as previously described[56]. To calculate total human leukemia cells engrafted within the total humanized ossicle-niche space, as compared to the mouse BM, the percentage of human CD45$^+$CD33$^+$ cells (determined by flow cytometry) was multiplied with the maximal number of cells recoverable from all the humanized ossicle-niche space (four ossicles combined) or the corresponding total mouse BM (for example, average total nucleated cells (TNC) in four ossicles: 5.83×10^7, $5.83 \times 10^7 \times 98.4\%$ (engraftment (%)) = 5.74×10^7 human leukemia cells.

Statistics. *P* values were calculated using nonparametric two-tailed Mann–Whitney test or unpaired Student's *t* test in Prism version 6 (GraphPad Software, Inc., La Jolla, CA). A *P* value of <0.05 was considered to be statistically significant. Limiting-dilution data are presented as the estimated limiting-dilution frequency ±95% confidence interval. Limiting-dilution analysis was done with the Extreme Limiting Dilution Analysis (ELDA) software provided by the Walter and Eliza Hall Institute of Medical Research Bioinformatics.

49. Alvarez, L.L. & Pardo, H.G. Guide for the care and use of laboratory animals — Natl-Res-Council. *Psicothema* **9**, 232–234 (1997).
50. Rohde, E., Schallmoser, K., Bartmann, C., Reinisch, A & Dirk, S. in *Pharmaceutical Manufacturing Handbook: Regulations and Quality* (ed. Gad, S.C.) 97–115 (John Wiley & Sons, Inc., 2008).
51. Schallmoser, K. *et al.* Rapid large-scale expansion of functional mesenchymal stem cells from unmanipulated bone marrow without animal serum. *Tissue Eng. Part C Methods* **14**, 185–196 (2008).
52. Dominici, M. *et al.* Minimal criteria for defining multipotent mesenchymal stromal cells. The International Society for Cellular Therapy position statement. *Cytotherapy* **8**, 315–317 (2006).
53. Notta, F. *et al.* Isolation of single human hematopoietic stem cells capable of long-term multilineage engraftment. *Science* **333**, 218–221 (2011).
54. Moraga, I. *et al.* Tuning cytokine receptor signaling by re-orienting dimer geometry with surrogate ligands. *Cell* **160**, 1196–1208 (2015).
55. Corces-Zimmerman, M.R., Hong, W.J., Weissman, I.L., Medeiros, B.C. & Majeti, R. Preleukemic mutations in human acute myeloid leukemia affect epigenetic regulators and persist in remission. *Proc. Natl. Acad. Sci. USA* **111**, 2548–2553 (2014).
56. Boggs, D.R. The total marrow mass of the mouse: a simplified method of measurement. *Am. J. Hematol.* **16**, 277–286 (1984).

doi:10.1038/nm.4103